

Seasonal climate summary southern hemisphere (autumn 2015): El Niño arrives

Alison Cook

Bureau of Meteorology, Melbourne, Australia

(Manuscript received November 2015; accepted December 2015)

Southern hemisphere circulation patterns and associated anomalies for the austral autumn 2015 are reviewed, with an emphasis on Pacific Basin climate indicators and Australian rainfall and temperatures. Autumn 2015 saw the development of El Niño, following a near-miss El Niño in 2014 that never quite met the thresholds needed to declare an event. Australia as a whole received about 20 per cent less rainfall than average for autumn, but tropical cyclone activity contributed to above average rainfall in western parts of Western Australia. Above average rainfall was also seen in some areas in the southern half of the country, while the north was drier than usual. The southwestern half of the continent experienced cooler than normal days, but in the northeastern half of Australia maximum temperatures were above average. A prolonged warm spell affected large parts of Australia during May.

Introduction

This summary reviews the southern hemisphere and equatorial climate patterns for autumn 2015, with particular attention given to the Australasian and Pacific regions. The main sources of information for this report are analyses prepared by the Bureau of Meteorology.

Pacific and Indian Basin climate indices

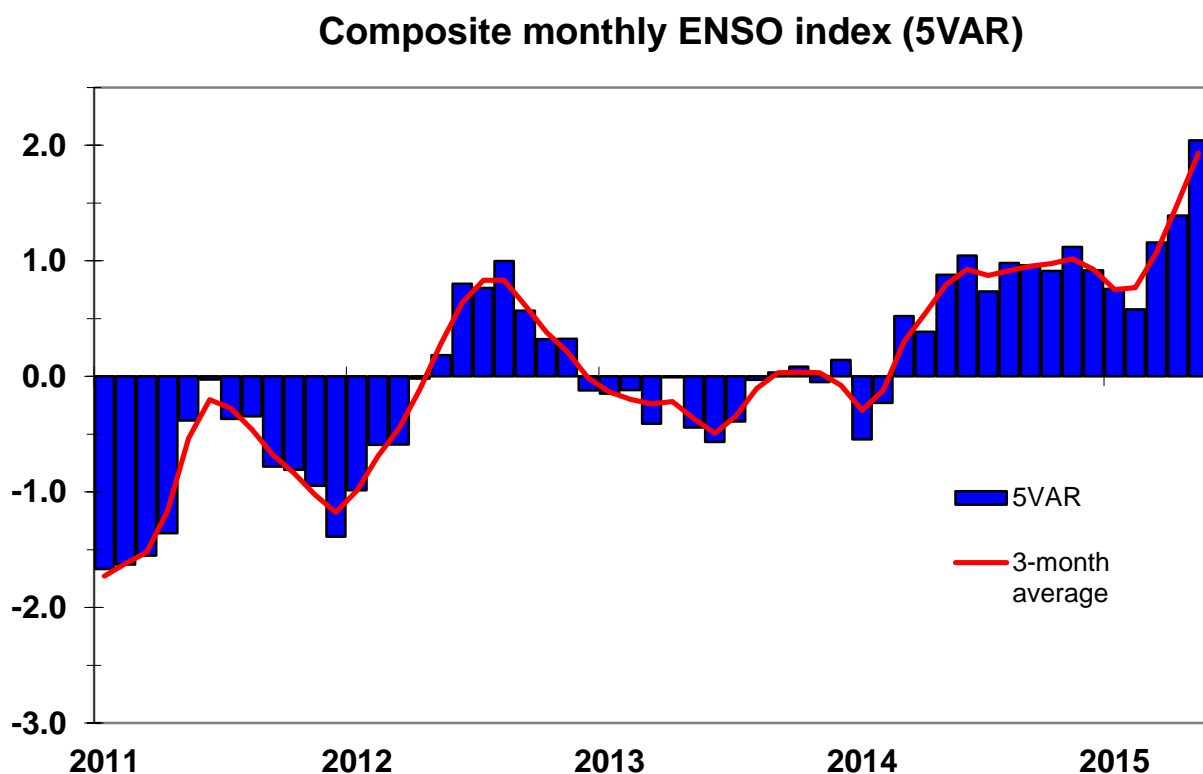
Southern Oscillation Index

The Troup Southern Oscillation Index¹ (SOI) for the period January 2011 to May 2015 is shown in Fig. 1, together with a five-month weighted moving average. From winter 2014 SOI values were predominantly negative, the only exception being a weakly positive monthly value of +0.6 for February 2015. Monthly values for autumn 2015 were -11.2 in March, -3.8 in April, and -13.7 in May, giving a seasonal average of -9.6. Autumn mean sea level pressure (MSLP) values for Darwin were 1.4 hPa above average at 1010.8 hPa, and very close to average at 1012.1 hPa for Tahiti. The monthly MSLP anomalies for March, April and May for Darwin were +1.3, +1.0 and +2.1 respectively, and at Tahiti, -0.8, +0.5 and +0.4. Positive MSLP anomalies at Darwin throughout the season are consistent with a drier than usual autumn for northern Australia (see rainfall section).

¹ The Troup Southern Oscillation Index (Troup 1965) used in this article is ten times the standardised monthly anomaly of the difference in mean sea level pressure (MSLP) between Tahiti and Darwin. The calculation is based on a sixty-year climatology (1933–1992). The Darwin MSLP is provided by the Bureau of Meteorology, with the Tahiti MSLP provided by Météo France inter-regional direction for French Polynesia.

The Multivariate ENSO Index⁵ (MEI), produced by the Physical Sciences Division of the Earth Systems Research Laboratory (formerly known as the US Climate Diagnostics Center), is derived from a number of atmospheric and oceanic parameters calculated as a two-month mean. As for 5VAR, significant positive anomalies are typically associated with El Niño, while large negative anomalies indicate La Niña. The 2015 February-March (0.65), March-April (0.95) and April-May (1.57) values of the MEI were all positive, and like the 5VAR index, showed an increasing trend throughout autumn 2015.

Figure 2 5VAR composite standardised monthly ENSO index from January 2011 to May 2015, together with a weighted three-month moving average. See text for details.



Outgoing long-wave radiation

Outgoing long-wave radiation (OLR) in the equatorial Pacific Ocean may be used as a proxy for tropical convection. Decreased OLR usually indicates increased convection (and associated cloudiness and rainfall), and increased OLR usually indicates decreased convection. During El Niño, increased convection, or decreased OLR, often occurs near the Date Line. The opposite is observed during La Niña.

NOAA's Climate Prediction Center computes standardised monthly OLR anomalies for the region from 5°S to 5°N and 160°E to 160°W⁶. In 2015, the monthly OLR anomaly values for March, April and May were -1.9, -1.1 and -1.0 respectively, and the seasonal average for autumn, -1.3; indicating increased convection near the Date Line.

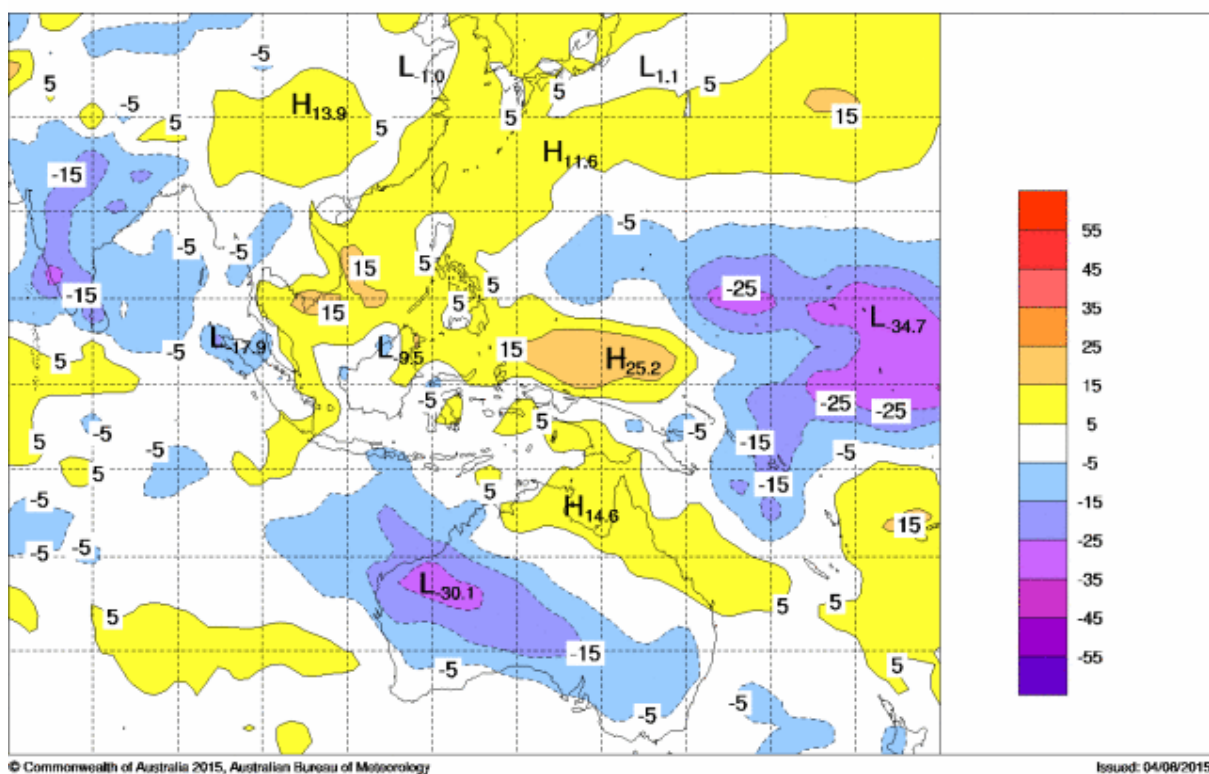
The spatial pattern of seasonal OLR anomalies across the Asia-Pacific region between 40°S and 40°N for autumn 2015 is shown in Fig. 3. In the Australian region, negative OLR anomalies were observed across the north west of Western Aus-

⁵ Multivariate ENSO Index obtained from <http://www.esrl.noaa.gov/psd/people/klaus.wolter/MEI/table.html>. The MEI is a standardised anomaly index described in Wolter and Timlin 1993, and 1998.

tralia, while positive anomalies (indicating reduced convection) were observed over the northern tropics of Australia. This region of positive anomalies extended north across parts of Indonesia and much of the western and northern Pacific. These differences were reflected in the rainfall totals for autumn; rainfall totals over northern Australia were generally below average, while areas of above average rainfall were observed over the southern half of the continent. An area of rainfall in the top decile (top 10% of records) was seen in the west of Western Australia, coinciding with significantly negative OLR anomalies (see Fig. 16). A large area of strongly negative OLR anomalies was observed over the equatorial Pacific on and to the west of the Date Line, consistent with conditions expected under El Niño.

Figure 3 OLR anomalies for autumn 2015 (Wm^{-2}). Base period is 1979–2000. The mapped region extends from 40°S to 40°N and 70°E to 180°E

OLR 2.5X2.5 NOAA REAL TIME-OLRAV (W/M^2) 20150301 0000 20150531 0000



Madden-Julian Oscillation (MJO)

The Madden-Julian Oscillation (MJO) is a tropical atmospheric anomaly which develops in the Indian Ocean and propagates eastwards into the Pacific Ocean (Madden and Julian 1971, 1972, and 1994). The MJO takes approximately 30 to 60 days to reach the western Pacific, with a frequency of six to twelve events per year (Donald et al, 2004).

When the MJO is in an active phase, it is associated with areas of increased and decreased tropical convection, with effects on the southern hemisphere mainly occurring during early autumn before transitioning to the northern hemisphere. A description of the Real-time Multivariate MJO (RMM) index and the associated phases can be found in Wheeler and Hendon (2004).

The phase-space diagram of the RMM for autumn 2015 is shown in Fig. 4, and the evolution of tropical convection anomalies along the equator with time is shown in Fig. 5. A strong MJO pulse occurred in early March, originating over the Maritime Continent (phase 4). It progressed towards the western Pacific (phases 6 and 7), moving across the western hemisphere and Africa (phases 8 and 1) and the Indian Ocean (phases 2 and 3), before decaying in early to mid-April. This

MJO pulse reached a record high amplitude of 4.03 on 16 March 2015 in the western Pacific. Prior to this event, the highest amplitude was recorded in February 1985 – the only other time since monitoring began in 1974 that the MJO amplitude has exceeded 4. Only weak MJO activity was seen during the second half of April and throughout May. In Fig. 5, the negative OLR anomalies in March between approximately 150°E and 180° correspond with the strong MJO pulse.

Figure 4 Phase-space representation of the MJO index for autumn 2015. Daily values are shown with March in red, April in green, and May in blue. The eight phases of the MJO and the corresponding (approximate) locations of the near-equatorial enhanced convective signal are labelled.

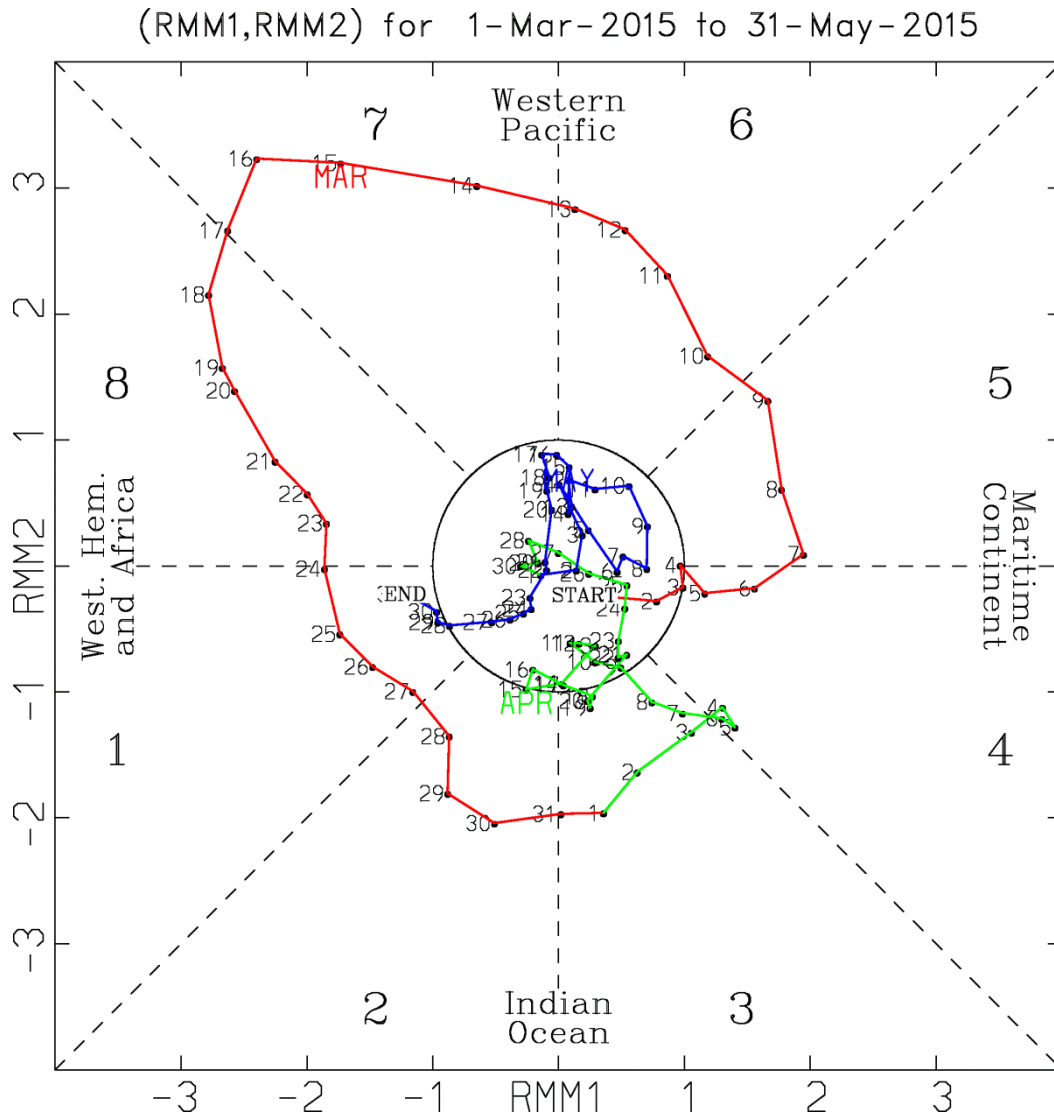
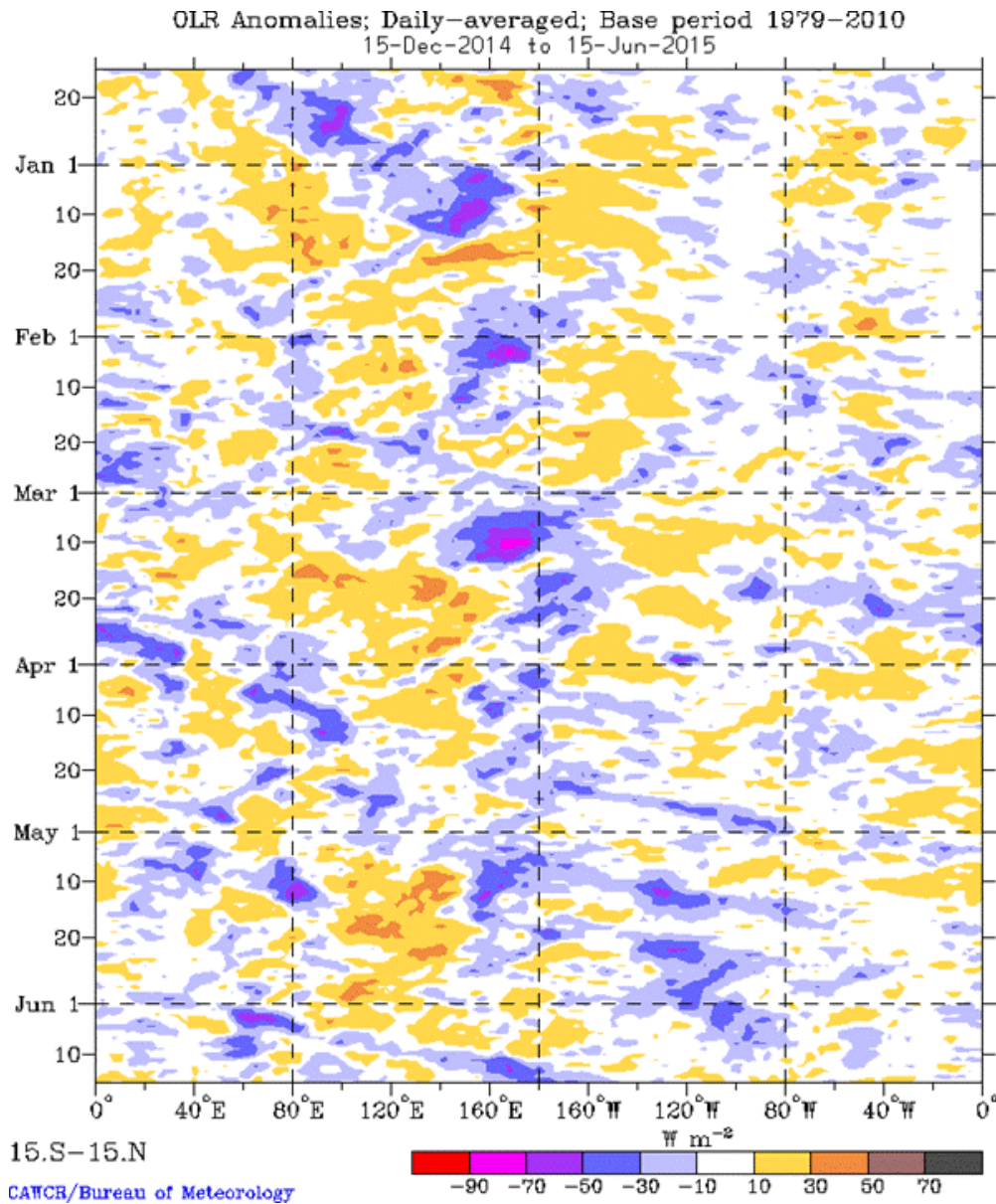


Figure 5 Time-longitude section of daily-averaged OLR anomalies, averaged for 15°S to 15°N, for the period December 2014 to June 2015. Anomalies are with respect to a base period of 1979–2010.



Oceanic patterns

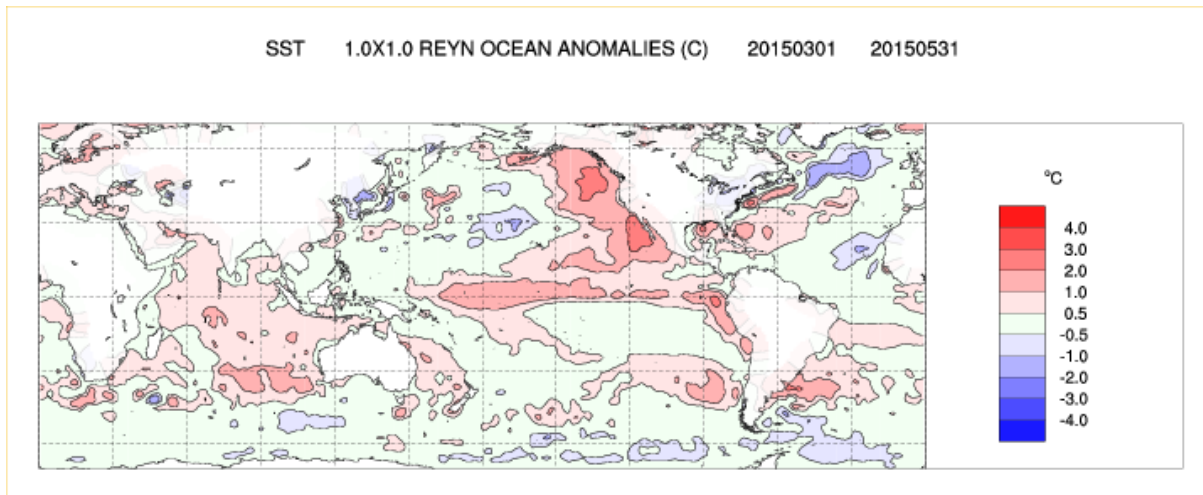
Sea surface temperatures (SSTs)

Autumn 2015 sea-surface temperature (SST) anomalies, obtained from the U.S. National Oceanic and Atmospheric Administration (NOAA) Optimum Interpolation analyses (Reynolds et al. 2002), are shown in Fig. 6. Negative (cool) anomalies are shown in blue, while positive (warm) anomalies are coloured red.

During summer 2014–15, SSTs across much the Pacific Ocean were warmer than average (Blockley 2015). Throughout autumn, SSTs warmed across the eastern equatorial Pacific Ocean, consistent with the development of an El Niño - temperatures along the equator from the Peruvian coast extending to the western edge of the maritime continent were anomalously warm. The monthly NINO3.4 index rose steeply from +0.57 °C in March to +1.06 °C in May. Other

anomalously warm regions included waters along the eastern Australian coast, and seas to the west and east of South America. Large areas of anomalously warm sea-surface temperatures were seen throughout the Indian Ocean during autumn 2015.

Figure 6 Anomalies of global SST for austral autumn 2015 (°C).



Equatorial Pacific sub-surface patterns

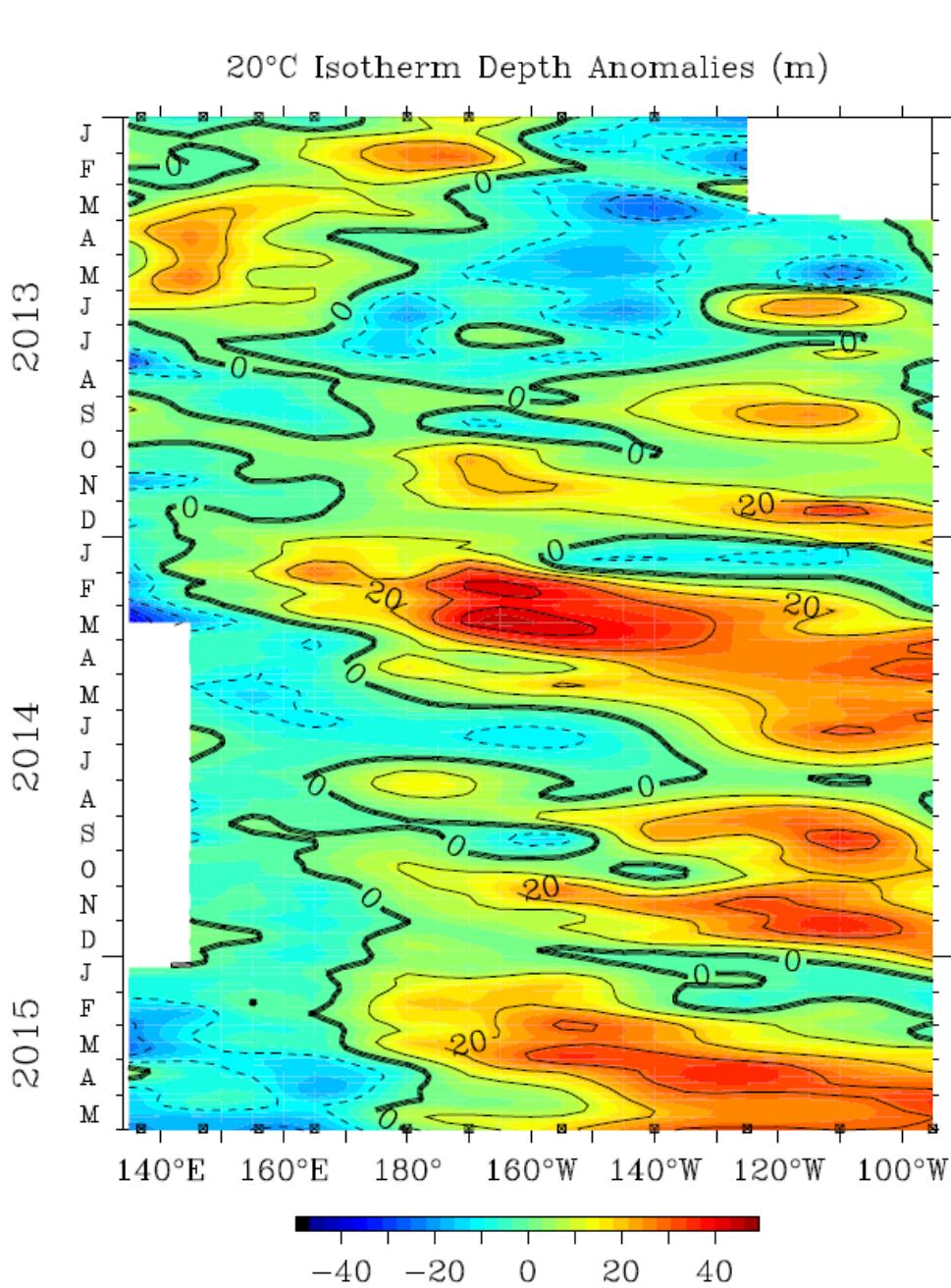
The Hovmöller diagram for the 20°C isotherm depth anomaly along the equator from January 2013 to May 2015, obtained from NOAA's TAO/TRITON data⁶ is shown in Fig. 7. The 20°C isotherm depth is generally located close to the equatorial thermocline, which is the region of greatest temperature gradient with depth, and is the boundary between the warm near-surface and cold deep-ocean waters. Therefore, measurements of the 20°C isotherm depth make a good proxy for the thermocline depth. Positive (negative) anomalies correspond to the 20°C isotherm being deeper (shallower) than average.

A deeper thermocline results in less cold water available for upwelling, and therefore a warming of surface temperatures. The converse is also true.

A significant deepening of the thermocline across the equatorial eastern Pacific Ocean was seen during autumn 2015.

⁶Hovmöller plot obtained from <http://www.pmel.noaa.gov/tao/jsdisplay/>

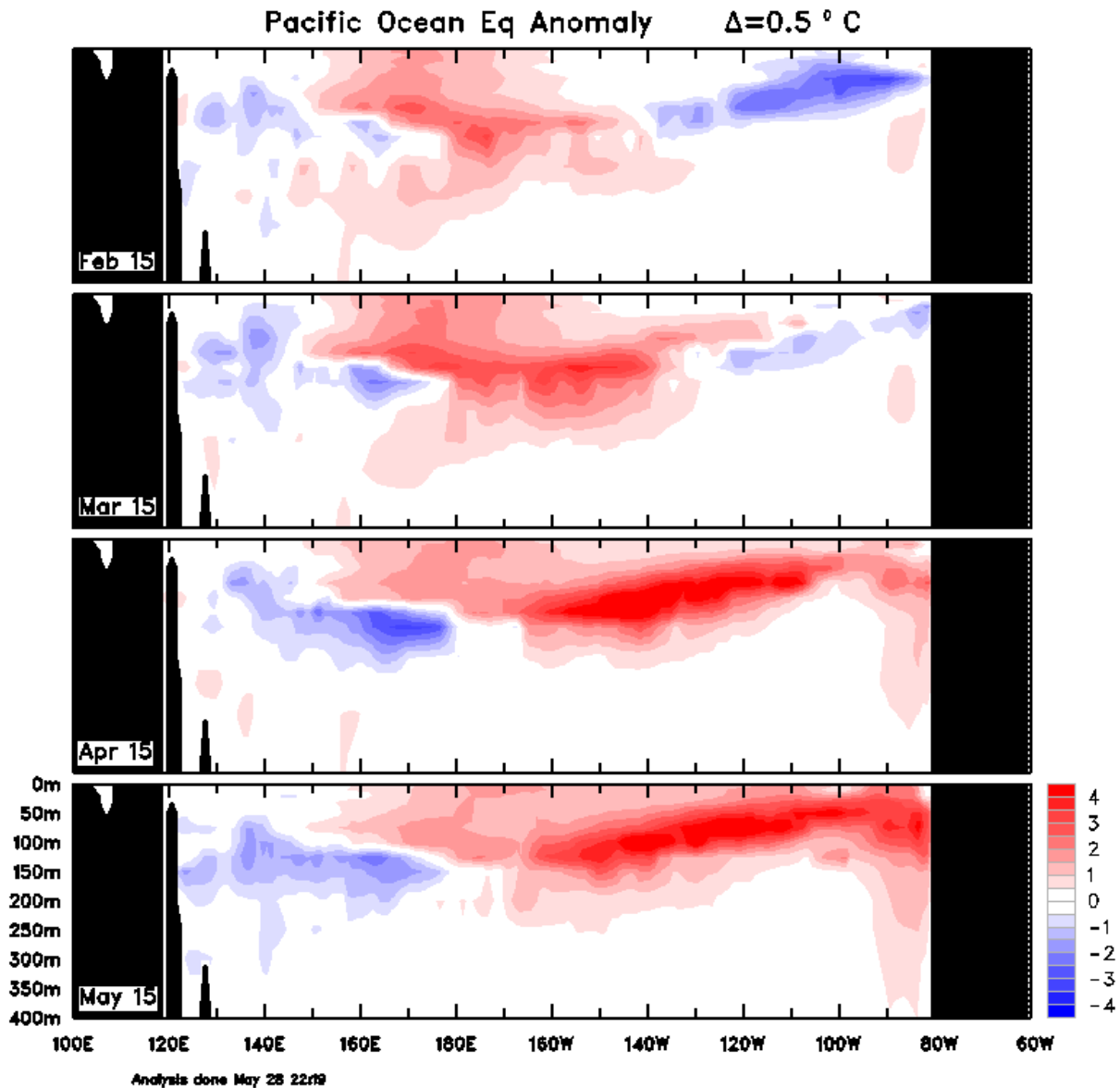
Figure 7 Time-longitude section of the monthly anomalous depth of the 20°C isotherm at the equator (2°S to 2°N) for January 2013 to May 2015. (Plot obtained from the TAO Project Office).



TAO Project Office/PMEL/NOAA

Fig. 8 shows a cross-section of monthly equatorial sub-surface analyses from February 2015 to May 2015. Red shading indicates positive (warm) anomalies, and blue shading indicates negative (cool) anomalies. In February 2015, warm sub-surface anomalies were present in the central Pacific Ocean, with cool anomalies in the east and west. The region of warm anomalies increased in size and strength and slowly moved eastwards during autumn 2015 whilst gradually migrating towards the surface.

Figure 8 Four-month sequence from February to May 2015 of vertical sea subsurface temperature anomalies at the equator for the Pacific Ocean. The contour interval is 0.5 °C. (Plot obtained from the Bureau of Meteorology⁷).



Atmospheric patterns

Surface analysis

The mean sea level pressure (MSLP) pattern for autumn 2015 is shown in Fig. 9, computed using data from the 0000 UTC daily analyses of the Bureau of Meteorology's Australian Community Climate and Earth System Simulator (ACCESS) model⁸. MSLP anomalies are shown in Fig. 10, relative to the 1979–2000 climatology obtained from the National Centers for Environmental Prediction (NCEP) II Reanalysis data (Kanamitsu et al. 2002). The MSLP anomaly field is not shown over areas of elevated topography (grey shading).

⁷ This and other analyses available from <http://www.bom.gov.au/oceanography/oceantemp/pastanal.shtml>

⁸ For more information on the Bureau of Meteorology's ACCESS model, see <http://www.bom.gov.au/nwp/doc/access/NWPData.shtml>

The autumn 2015 MSLP pattern was zonal around Antarctica, with the subtropical ridge forming a band of high pressure at around 30°S. A centre of high pressure was located over the Great Australian Bight (1023.1 hPa) as part of a band that extended west to another high pressure centre over the southern Indian Ocean (1023.6 hPa). Additional high pressure centres were located over the southern South Atlantic west of the Cape of Good Hope (approximately 1020 hPa) and to the west of Chile (approximately 1019 hPa). The region of lowest pressure was located just off the coast of Antarctica, at around 120°E (976.9 hPa).

Figure 9 Autumn 2015 MSLP (hPa). The contour interval is 5 hPa.

MSLP 2.5X2.5 ACCESS OP. ANAL. (hPa) 20150301 0000 20150531 0000

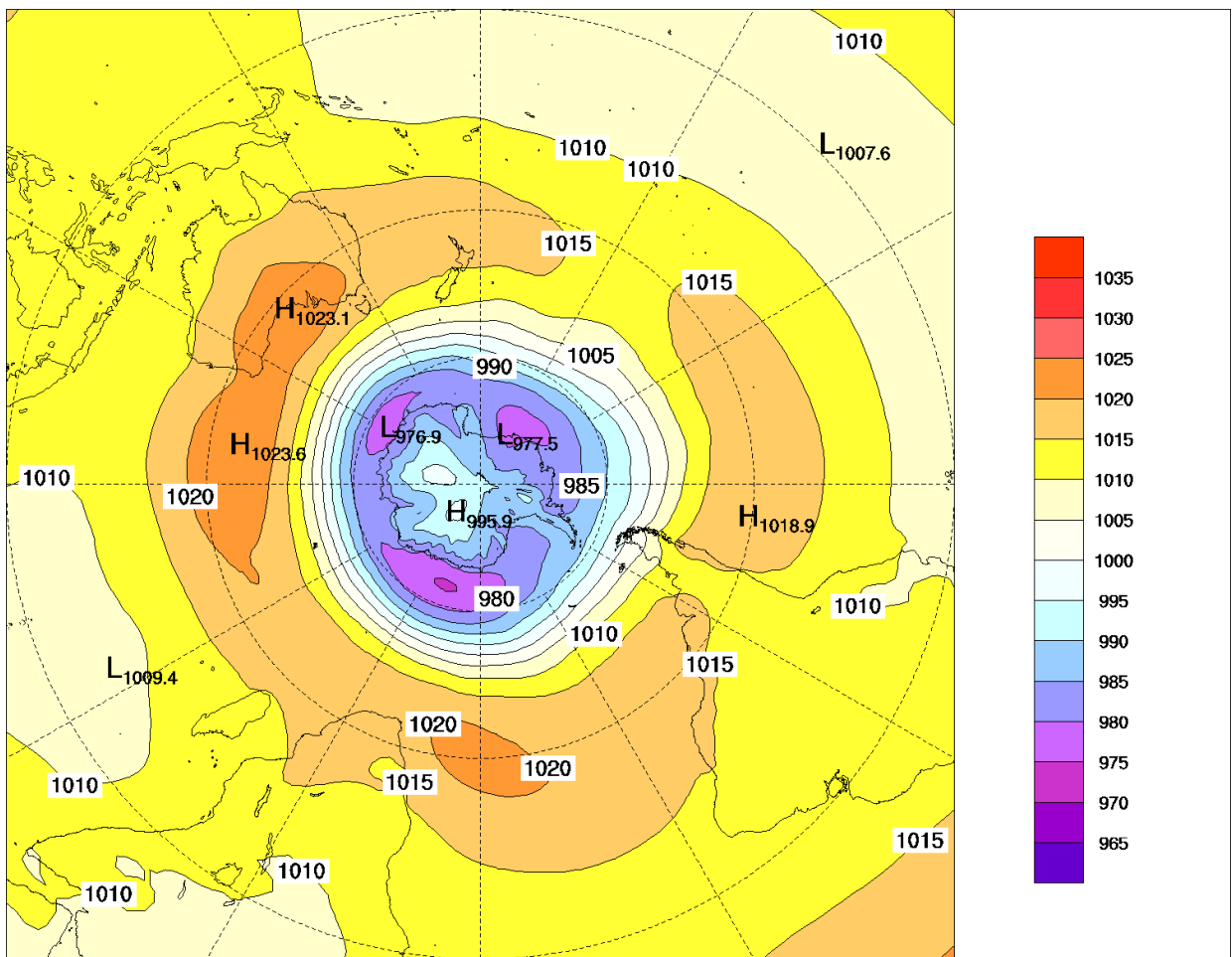
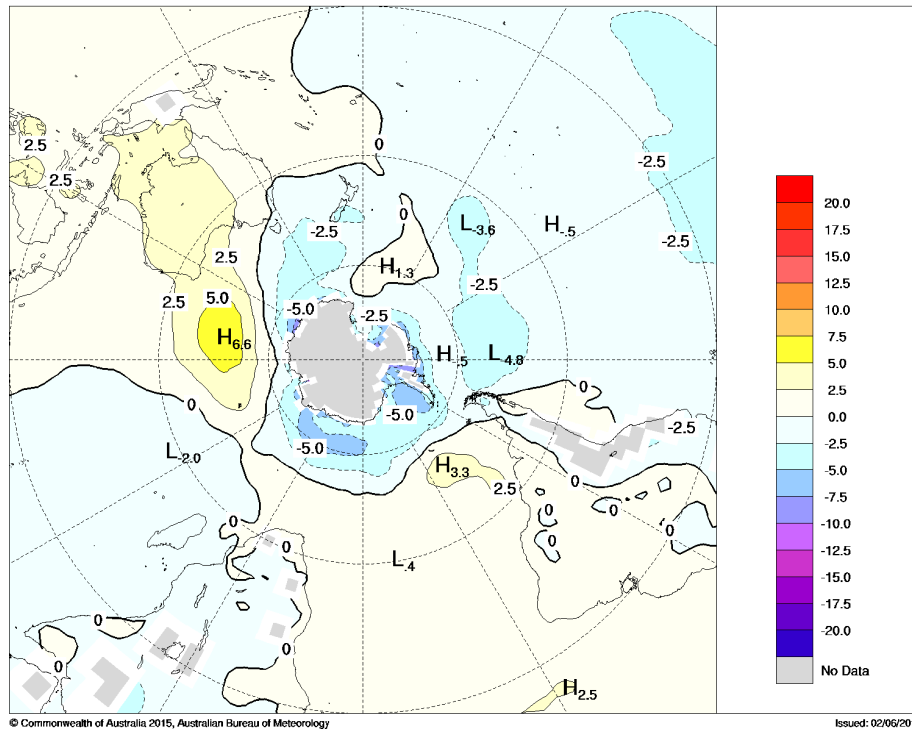


Figure 10 Autumn 2015 MSLP anomalies (hPa), from a 1979–2000 climatology.

MSLP 2.5X2.5 ACCESS OP. ANAL.-NCEP2 (hPa) 20150301 0000 20150531 0000



The most significant high pressure anomaly (+6.6 hPa) was seen over the southern Indian Ocean at around 105°E, though high pressure anomalies were observed over all of western and central Australia. Low pressure anomalies were evident in areas of the southern Pacific Ocean and throughout most of the area south of 60°S, with the most significant (lower than -5.0 hPa) anomalies seen in three locations just off the coast of Antarctica.

Mid-tropospheric analyses

The 500 hPa geopotential height, an indicator of the steering of surface synoptic systems across the southern hemisphere, is shown for autumn 2015 in Fig. 11. The associated anomalies are shown in Fig. 12. The autumn 500 hPa geopotential height field was dominated by zonal flow, with three weak troughs located south of the Great Australian Bight (~130°E), in the eastern Pacific (~100°W), and to the west of South Africa (~0°). Geopotential height anomalies generally followed a similar pattern to the MSLP anomalies (Fig. 10) in the Australian region; positive geopotential height anomalies were seen over the southern Indian Ocean at around 105°E, and more broadly over the Australian continent. A band of negative geopotential height anomalies occurred around the eastern coastline of Antarctica, and over the Pacific ocean just to the west of South America at about 50°S.

Figure 11 Autumn 2015 500 hPa mean geopotential height (gpm).

Z0500 2.5X2.5 ACCESS OP. ANAL. (M) 20150301 0000 20150531 0000

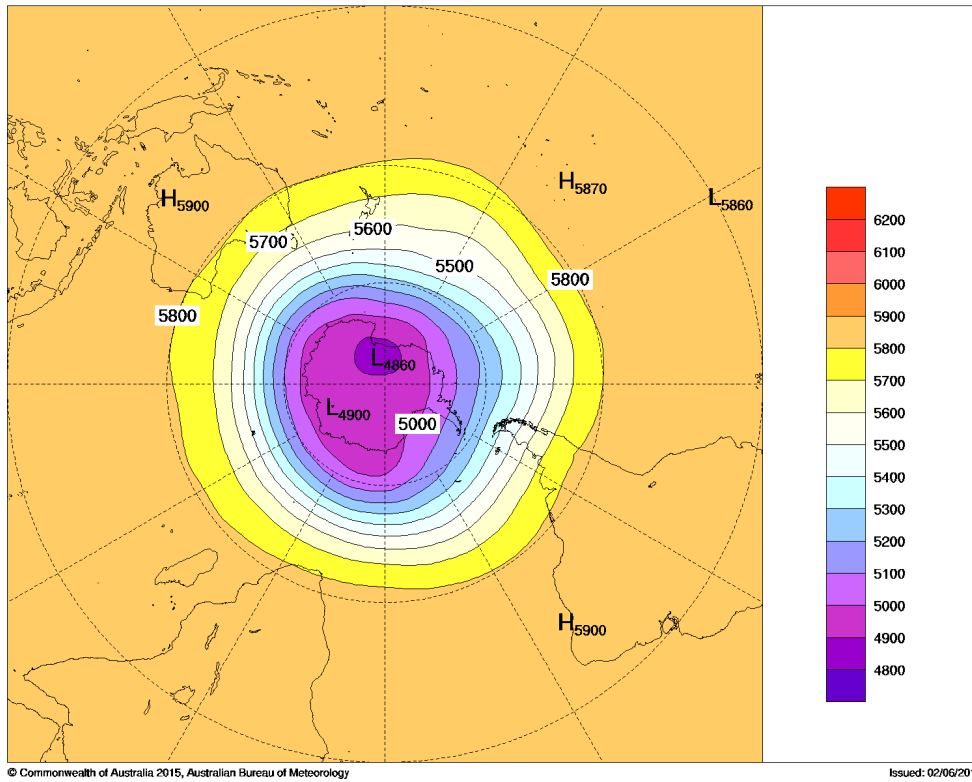
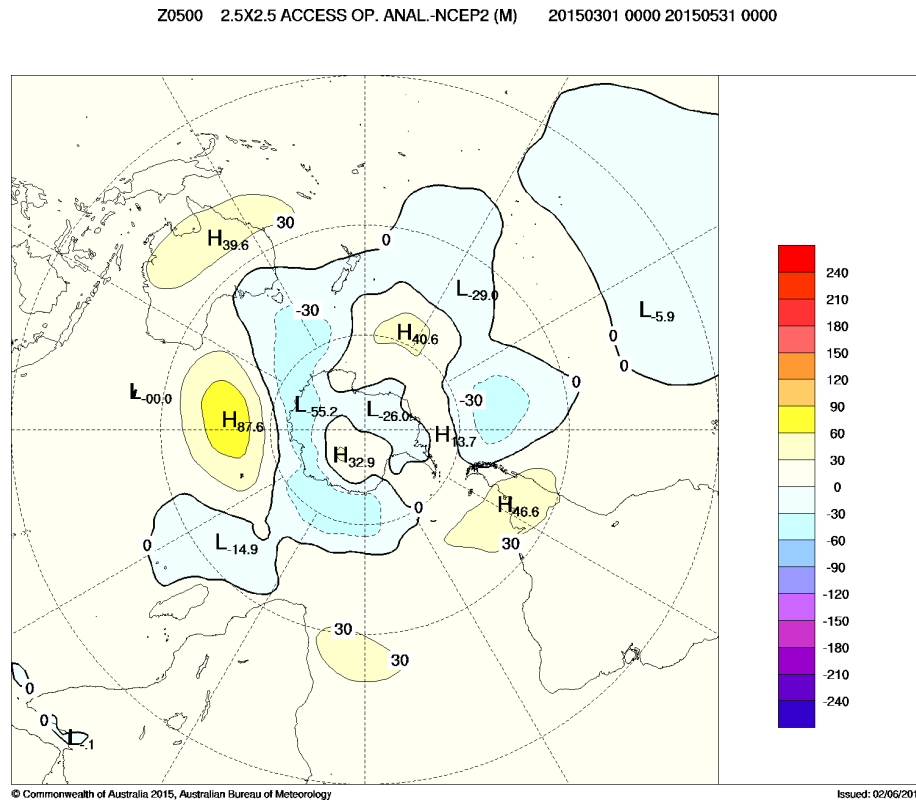


Figure 12 Autumn 2015 500 hPa mean geopotential height anomalies (gpm), from a 1979–2000 climatology.

Southern Annular Mode (SAM)

The Southern Annular Mode (SAM, also known as the Antarctic Oscillation or AAO) describes the periodic, approximately 10 day oscillation of atmospheric pressure between the polar and mid-latitude regions of the southern hemisphere. Positive phases of the SAM are characterised by increased mass over the mid-latitudes and decreased mass over Antarctica (that is, anomalously high pressure over the mid-latitudes and anomalously low pressure over Antarctica), and an associated poleward contraction in the belt of westerly winds that circles Antarctica. Conversely, negative phases of the SAM related to decreased mass (lower pressure) over the mid-latitudes, and increased mass over Antarctica, with an equatorward expansion of the mid-latitude westerly wind belt. A similar oscillation occurs in the northern hemisphere, the Northern Annular Mode or NAM (also known as the Arctic Oscillation or AO).

The Climate Prediction Center produces a standardised monthly SAM index⁹. The March, April and May values for 2015 were +0.77, +1.03 and +0.42 respectively, with an overall autumn value of +0.74. In autumn and winter, a positive SAM is associated with decreased rain over southern Australia due to a southward contraction of the storm track, however the impact during autumn is generally weaker than during winter (see Hendon et al, 2007).

The MSLP anomaly chart (Fig. 10) shows anomalously low pressure over Antarctica, and higher pressure in some parts of the mid-latitude region, particularly over the Australian region and to the southwest of Australia. This is consistent with the positive seasonal value of the SAM.

⁹ Climate Prediction Center (NOAA) monthly mean Antarctic Oscillation (AAO, or SAM) index since January 1979 http://www.cpc.ncep.noaa.gov/products/precip/CWlink/daily_ao_index/ao/ao.shtml

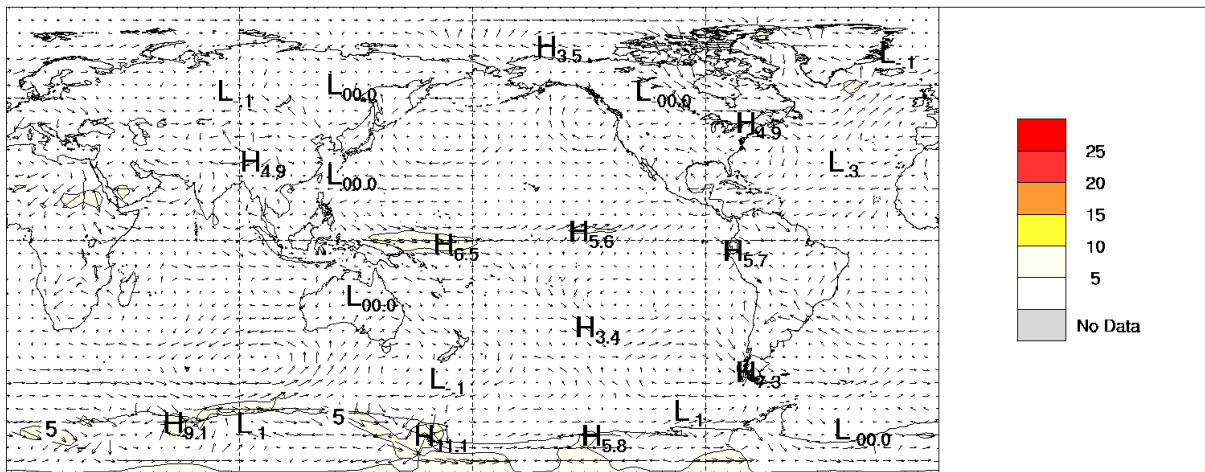
Winds

Figures 13 and 14 show autumn 2015 low-level (850 hPa) and upper-level (200 hPa) wind anomalies respectively (winds computed from ACCESS and anomalies with respect to the 22-year NCEP climatology). Isotach contours are at 5 ms⁻¹ intervals. In general, low-level 850 hPa anomalies for autumn 2015 were within 5 ms⁻¹ of the long term average. Slightly stronger anomalies (up to 10 ms⁻¹) in a westerly direction are seen in the western tropical Pacific Ocean, conditions consistent with the development of El Niño.

The upper level (200 hPa) wind anomaly chart shows westerly winds across southern Australia and in a band at around 40°S extending across the Pacific Ocean. Westerly anomalies were also apparent over parts of the Southern Ocean, and across several areas in the northern hemisphere. A band of easterly wind anomalies was present over the central and western Pacific Ocean, just north of the equator.

Figure 13 Austral autumn 2015 850 hPa vector wind anomalies (ms⁻¹).

|V|0850 2.5X2.5 ACCESS OP. ANAL.-NCEP2 (M/S) 20150301 0000 20150531 0000

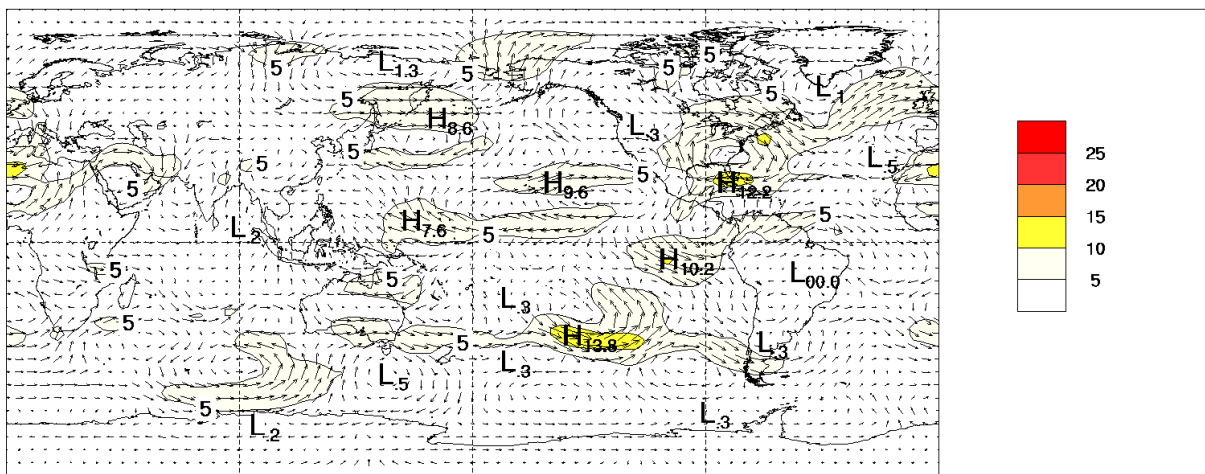


© Commonwealth of Australia 2015, Australian Bureau of Meteorology

Issued: 02/06/2015

Figure 14 Austral autumn 2015 200 hPa vector wind anomalies (ms⁻¹).

|V|0200 2.5X2.5 ACCESS OP. ANAL.-NCEP2 (M/S) 20150301 0000 20150531 0000



© Commonwealth of Australia 2015, Australian Bureau of Meteorology

Issued: 02/06/2015

Australian region

Rainfall

Rainfall totals (Fig. 15) and deciles (Fig. 16) show that much of northern Australia was drier than normal during autumn 2015. Conversely, much of western and central Western Australia received higher than average rainfall totals, with some areas experiencing rainfall that was in the top decile (top 10%) - deciles are calculated using gridded rainfall data for all autumn periods between 1900 and 2015. Across southeastern Australia results were mixed: many areas received near-average rainfall, with some regions locally receiving above or below average totals (Figure 16).

A summary of seasonal rainfall ranks and extremes is shown in Table 1 for each State and Territory. Percentage areas of rainfall in different categories (e.g. highest and lowest on record) are shown for each State and Territory in Table 2. Averaged across Australia, autumn rainfall was below normal with an area-averaged value of 96.6 mm, which is about 20 per cent below the 1961-1990 average of 120.5 mm (see Table 1). Autumn 2015 was particularly dry in Queensland and the Northern Territory, where rainfall was 48 and 61 per cent below average respectively. In comparison, rainfall was six per cent above average in Tasmania and 38 per cent above average in Western Australia.

Autumn rainfall was in the highest decile (wettest ten per cent of years) over 7.8 per cent of the country, mostly in central and western Western Australia but with small areas in New South Wales and South Australia. Specifically, 22.6 per cent of Western Australia, 2.5 per cent of New South Wales and 1.2 per cent of South Australia received rainfall in the highest decile. In contrast, 6.1 per cent of Australia recorded rainfall in the lowest decile (driest ten per cent of years) for autumn 2015, 17.5 per cent of the Northern Territory and 13.2 per cent of Queensland.

March saw below-average rainfall for Australia (26.0 per cent below average), with above average falls only occurring in northern and western Tasmania and over Western Australia. In April, rainfall was closer to average Australia-wide (-8.5 per cent), but varied considerably across the country – Queensland, Tasmania and the Northern Territory saw significantly below average rainfall, whereas totals were above average across all other states. In May, nationally-averaged rainfall was 18.7 per cent below average, with near-average falls in South Australia and Western Australia, above average totals in Tasmania, and below average rainfall everywhere else.

Four cyclones occurred in the Australian region during autumn 2015: *Nathan*, *Olwyn*, *Ikola* and *Quang*. *Ikola* was located to the west of Australia, and did not make landfall. *Nathan* began as a tropical low in the Coral Sea, before intensifying and being named as a category 1 cyclone on 10 March. It remained over the ocean for the next 10 days while slowly intensifying, before crossing the Cape York Peninsula coast as a category 4 cyclone in the early hours of March 20. *Nathan* then continued westward, bringing heavy rain and flooding to many parts of the Northern Territory's Top End. *Olwyn* and *Quang* impacted Western Australia's northern west coast; with *Olwyn* causing minor to moderate damage in west Pilbara and west Gascoyne communities.

Figure 15 Autumn 2015 rainfall totals (mm) for Australia.

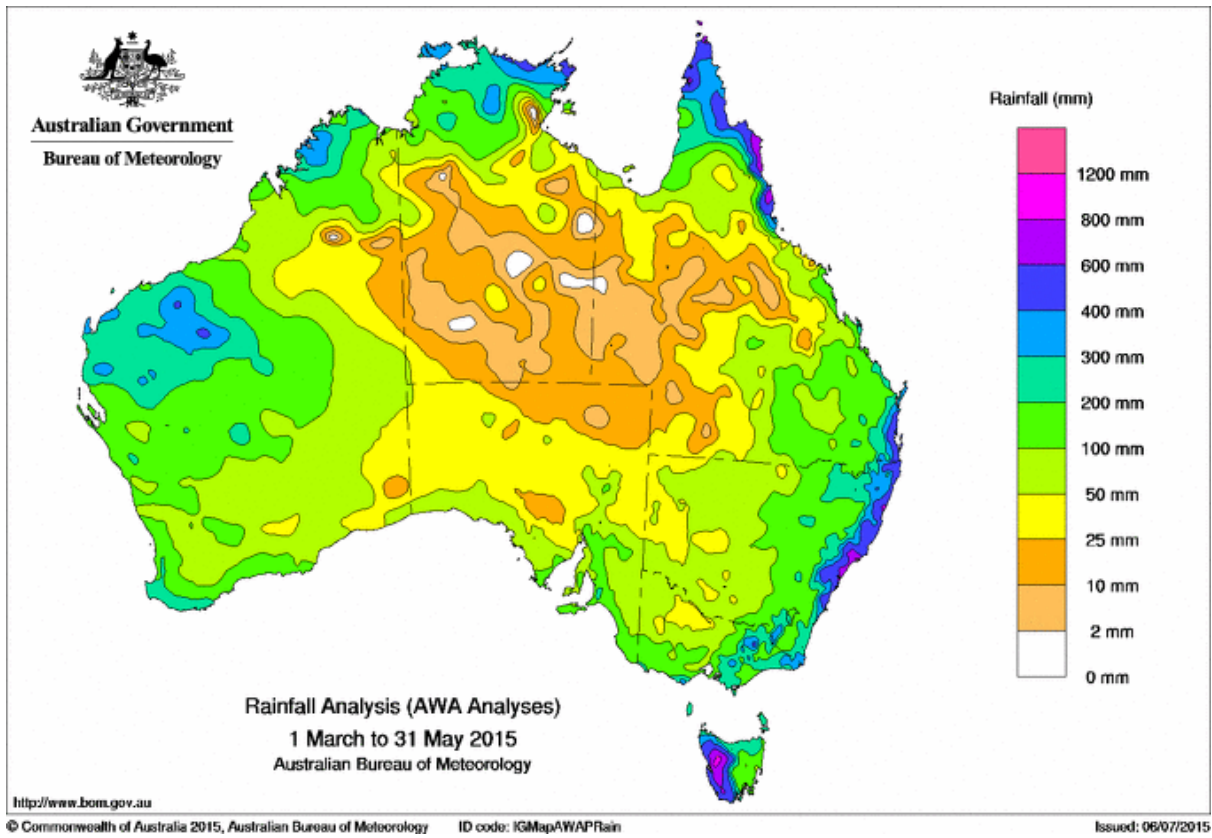


Figure16 Autumn 2015 rainfall deciles for Australia: decile ranges based on grid-point values over all autumns from 1900 to 2015.

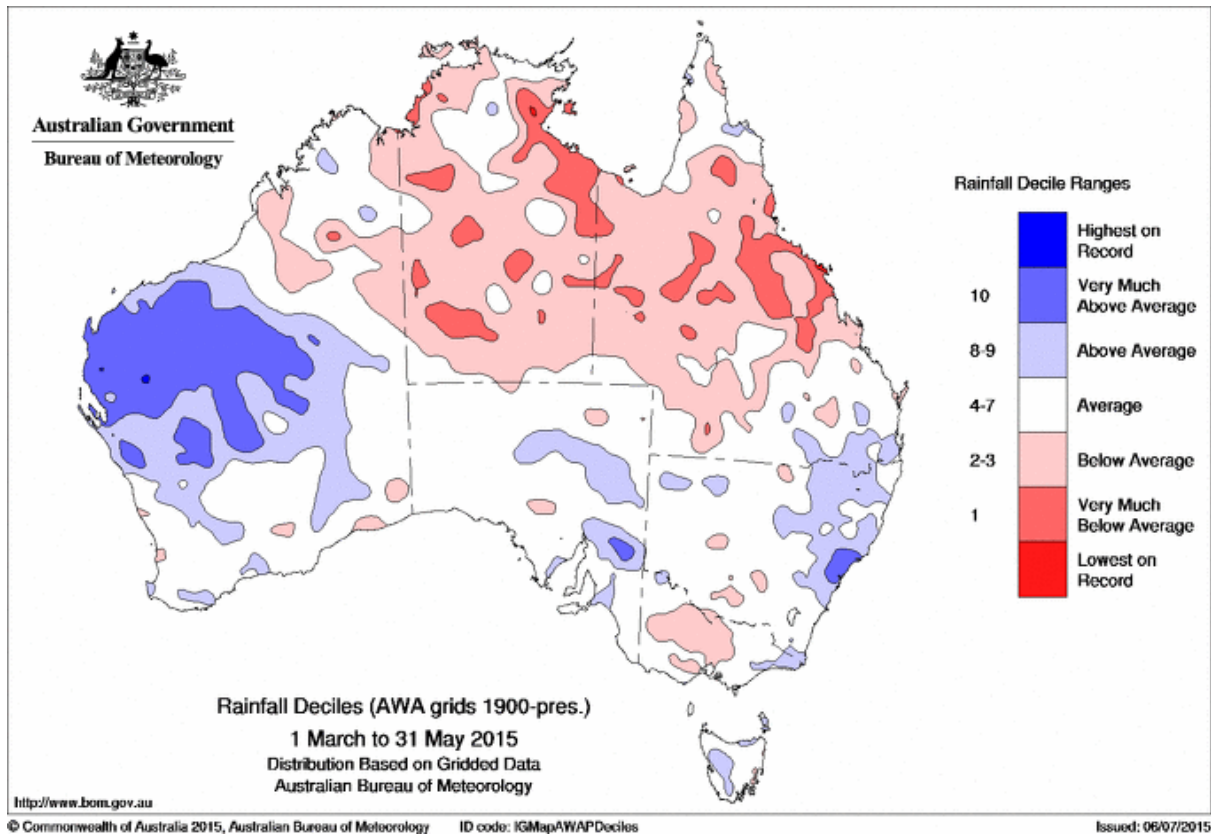


Table 1 Summary of the seasonal rainfall ranks and extremes on a national and State basis for autumn 2015. The ranking in the 2nd last column goes from 1 (lowest) to 116 (highest) and is calculated over the years 1900 to 2015 inclusive.

<i>Region</i>	<i>Highest seasonal total (mm)</i>	<i>Lowest seasonal total (mm)</i>	<i>Highest daily total (mm)</i>	<i>Area-averaged rainfall (mm)</i>	<i>Rank of area-averaged rainfall</i>	<i>% difference from mean</i>
Australia	1602.8 at Belenden Ker Top Station (Qld)	0.0 at multiple locations	307.5 at Maitland Belmore Bridge (Hunter River) on 22 April	96.6	40	-20
Queensland	1602.8 at Belenden Ker Top Station	0.0 at multiple locations	286.6 at Mango Hill on 2 May	84.3	18	-48
New South Wales	936.4 at Yarras (Mount Seaview)	26.6 at Wanaaring (Ourimbah)	307.5 at Maitland (Belmore Bridge) on 22 April	136.9	79	-4
Victoria	693.6 at Haines Junction (Mount Sabine)	29.7 at Lake Boga (Kunat)	121.0 at Buchan (Snowy River/Basin Creek) on 8 April	130.3	49	-17

Tasmania	1218.2 at Mount Read	69.4 at Tunbridge (Austin-Vale)	106.0 at Mount Wellington (The Springs) on 15 May	361.5	83	+6
South Australia	346.4 at Piccadilly (Mount Lofty Botanic Garden)	8.2 at Tiewon	112.4 at Quorn on 17 April	45.7	64	-19
Western Australia	393.6 at Learmonth	20.8 at Argyle Aerodrome	134.0 at Mundabullangana on 28 May	124.5	94	+38
Northern Territory	707.0 at Nhulunbuy	0.0 at multiple locations	260.8 at Fanny Creek on 25 March	54.5	13	-61

Table 2 Percentage areas in different categories for autumn 2015 rainfall. ‘Severe deficiency’ denotes rainfall at or below the 5th percentile. Areas in decile 1 include those in ‘severe deficiency’, which in turn includes areas which are ‘lowest on record’. Areas in decile 10 include areas which are ‘highest on record’. Percentage areas of highest and lowest on record are given to two decimal places because of the small quantities involved; other percentage areas are to one decimal place.

<i>Region</i>	<i>Lowest on record (%)</i>	<i>Severe deficiency (%)</i>	<i>Decile 1 (%)</i>	<i>Decile 10 (%)</i>	<i>Highest on record (%)</i>
Australia	0.07	1.5	6.1	7.8	0.06
Queensland	0.13	2.8	13.2	0	0.00
New South Wales	0.00	0	0	2.5	0.00
Victoria	0.00	0	0	0	0.00
Tasmania	0.00	0	0	0	0.00
South Australia	0.00	0	0	1.2	0.00
Western Australia	0.00	0.1	0.2	22.6	0.20
Northern Territory	0.23	4.6	17.5	0	0.00

Table 3 Summary of the seasonal maximum temperature ranks and extremes on a national and State basis for autumn 2015. The ranking in the last column goes from 1 (lowest) to 106 (highest) and is calculated over the years 1910 to 2015 inclusive¹⁰.

<i>Region</i>	<i>Highest seasonal mean maximum (°C)</i>	<i>Lowest seasonal mean maximum (°C)</i>	<i>Highest daily temperature (°C)</i>	<i>Lowest daily maximum temperature (°C)</i>	<i>Area-averaged temperature anomaly (°C)</i>	<i>Rank of area-averaged temperature anomaly</i>
Australia	37.0 at Wyndham Aero	7.4 at Mount Wellington	46.5 at Birdsville on 19 March	-2.9 at Thredbo AWS on 13 May	+0.02	57
Queensland	36.1 at Century Mine	21.5 at Applethorpe	46.5 at Birdsville on 19 March	11.3 at Stanthorpe on 21 April	+1.29	98
New South Wales	28.6 at Mungindi	8.2 at Thredbo AWS	42.9 at Bourke on 3 March and at Mungindi on 20 March	-2.9 at Thredbo AWS on 13 May	+0.18	65
Victoria	23.3 at Mildura	7.8 at Mount Hotham	40.3 at Mildura on 19 March	-2.0 at Mount Hotham on 13 May	-0.53	37 (tied)
Tasmania	18.1 at Launceston (Ti Tree Bend)	7.4 at Mount Wellington	28.0 at Flinders Island Airport on 1 April	0.0 at Mount Wellington on 6 May and on 31 May	-0.83	25
South Australia	28.0 at Moomba	15.5 at Mount Lofty	45.4 at Moomba on 19 March	8.4 at Mount Lofty on 21 May	-0.76	22
Western Australia	37.0 at Wyndham Aero	20.3 at Shannon	44.3 at Roebourne Aero on 22 March	11.6 at Mount Barker on 4 May	-0.92	11
Northern Territory	36.8 at Bradshaw	27.2 at Arltunga	43.4 at Curtin Springs on 19 March and at Jervis on 3 March	14.7 at Arltunga on 14 May	+0.77	83.5 (tied)

¹⁰ A subset of the full temperature network is used to calculate the spatial averages and rankings shown in Table 2 (maximum temperature) and Table 3 (minimum temperature); this dataset is known as ACORN-SAT (see <http://www.bom.gov.au/climate/change/acorn-sat/> for details). These averages are available from 1910 to the present. As the anomaly averages in the tables are only retained to two decimal places, tied rankings are possible. Rankings marked with "=" denote tied rankings.

Table 4 Summary of the seasonal minimum temperature ranks and extremes on a national and State basis for autumn 2015. The ranking in the last column goes from 1 (lowest) to 105 (highest) and is calculated over the years 1910 to 2015 inclusive.

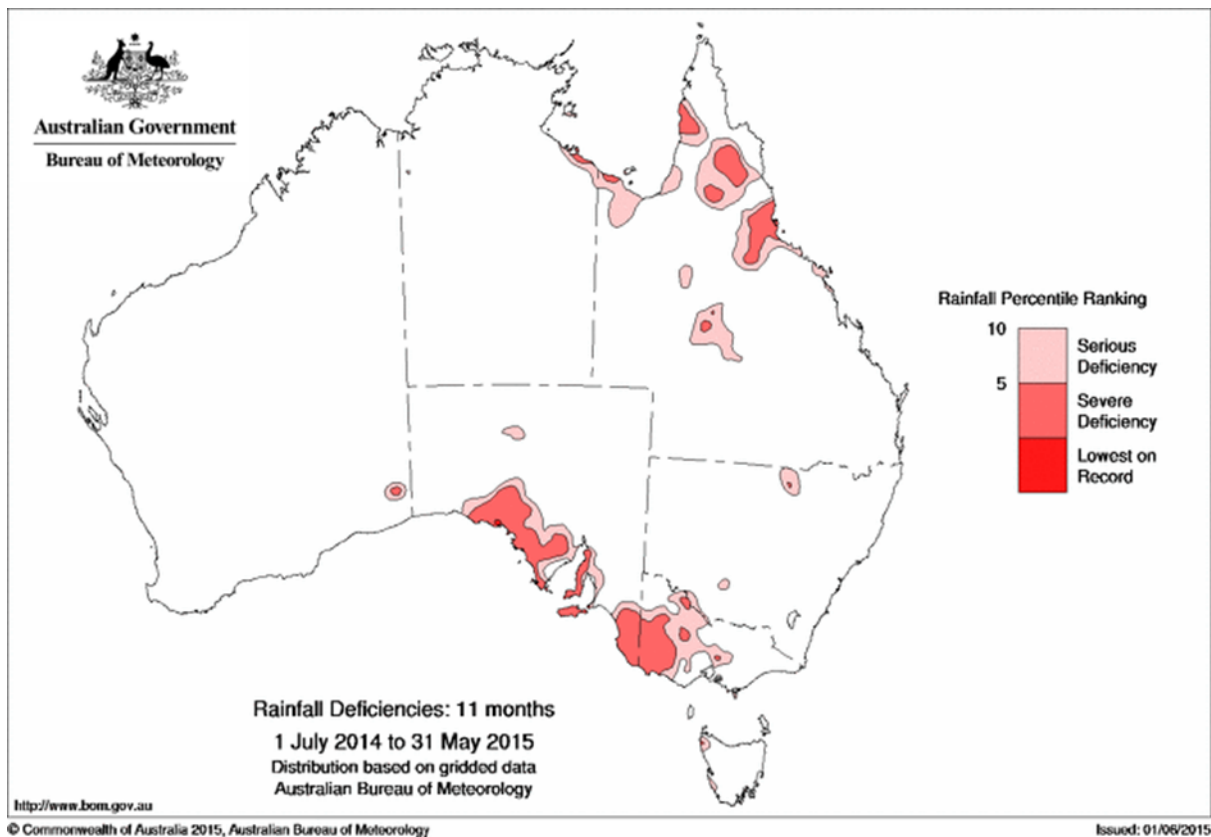
<i>Region</i>	<i>Highest seasonal mean minimum (°C)</i>	<i>Lowest seasonal mean minimum (°C)</i>	<i>Highest daily minimum temperature (°C)</i>	<i>Lowest daily temperature (°C)</i>	<i>Area-averaged temperature anomaly (°C)</i>	<i>Rank of area-averaged temperature anomaly</i>
Australia	27.4 at Browse Island	0.7 at Liawenee	31.9 at Boulia on 5 March	-8.9 at Cooma Airport on 24 May	-0.09	63
Queensland	25.4 at Coconut Island	9.9 at Applethorpe	31.9 at Boulia on 5 March	-2.3 at Applethorpe on 15 May	+0.46	88 (tied)
New South Wales	18.0 at Cape Byron	1.2 at Perisher Valley and Thredbo AWS	27.5 at Lightning Ridge on 04 March	-8.9 at Cooma Airport on 24 May	+0.41	83
Victoria	13.1 at Gabo Island	1.9 at Mount Hotham	19.0 at Rutherglen Research on 01 March	-6.5 at Omeo on 24 May	-0.46	53.5 (tied)
Tasmania	12.3 °C at Hogan Island	0.7 at Liawenee	18.4 at Flinders Island Airport on 18/03	-7.9 at Liawenee on 24 May	-0.75	25.5 (tied)
South Australia	15.0 at Moomba	7.0 at Coonawarra	27.8 at Moomba on 20 March	-1.6 at Padthaway South on 20 April	-0.46	41
Western Australia	27.4 at Browse Island	8.2 at Wandering	29.8 at Argyle Aerodrome on 15 March and at Wittenoom on 21 March	-2.5 at Eyre on 14 May	-0.2	52

Table 5 Percentage areas in different categories for autumn 2015. Areas in decile 1 include those which are ‘lowest on record’. Areas in decile 10 include those which are ‘highest on record’. Percentage areas of highest and lowest on record are given to two decimal places because of the small quantities involved; other percentage areas are given to one decimal place. Grid point deciles calculated with respect to 1911-2015.

Region	<i>Maximum Temperature</i>				<i>Minimum Temperature</i>			
	Lowest on record	Decile 1	Decile 10	Highest on record	Lowest on records	Decile 1	Decile 10	Highest on record
Australia	1.41	13.5	16	2.66	0.00	1.3	1.6	0.00
Queensland	0.00	0	46.6	8.63	0.00	0	4.7	0.00
New South Wales	0.00	0	0	0.00	0.00	0	1.2	0.00
Victoria	0.00	0.8	0	0.00	0.00	0.3	0	0.00
Tasmania	0.00	0	0	0.00	0.00	0.9	0	0.00
South Australia	0.00	16.2	0	0.00	0.00	1.3	0	0.00
Western Australia	4.30	34.7	2.6	0.00	0.00	0.7	1.2	0.00
Northern Territory	0.00	0	26.9	4.11	0.00	4.9	0	0.00

Drought

Areas of South Australia, western Victoria and Queensland continued to experience rainfall deficiencies during autumn 2015. Below average rainfall in autumn 2015 increased areas of serious and severe rainfall deficiency in Queensland. The 11-month period between August 2014 and May 2015 saw severe deficiencies across southern South Australia, western Victoria and in northern and central Queensland (Fig. 17).

Figure 17 Rainfall deficiencies for the 11-month period 1 July 2014 to 31 May 2015

Temperature

Figures 18 and 20 show the maximum and minimum temperature anomalies (relative to 1961-1990) for autumn 2015. Figures 19 and 21 respectively show the corresponding temperature deciles for maximum and minimum temperatures during autumn 2015, calculated using monthly temperature analyses from 1911 to 2015. A summary of maximum and minimum temperature deciles is shown in Table 5, and ranks and extremes in Tables 3 and 4.

The nationally-averaged maximum temperature for autumn 2015 was just 0.02 °C above average, though autumn average maximum temperatures varied widely across the country. In general, maximum temperatures were below average across the southwestern half of Australia, but above average across the northeastern half of the continent (see Fig. 18 and Fig. 19). Temperatures were more than 1 °C above average over large parts of Queensland and the Northern Territory, and more than 1 °C below average over much of Western Australia and South Australia. 46.6 per cent of Queensland was in the highest decile, while 34.7 per cent of Western Australia was in the lowest decile.

The nationally-averaged minimum temperature for autumn 2015 was slightly below average (0.09 °C below average). Queensland and New South Wales experienced above average night time temperatures, with all other States and Territories recording below average minimum temperatures.

Figure 18 Autumn 2015 maximum temperature anomalies (°C).

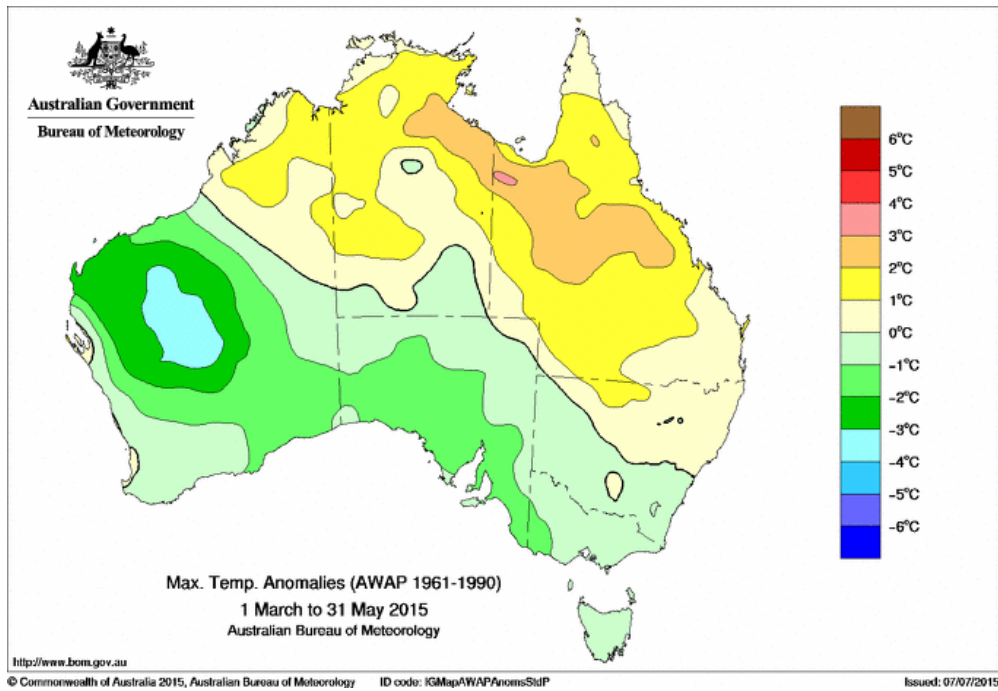


Figure 19 Autumn 2015 maximum temperature deciles: decile ranges based on grid-point values for all autumns from 1911 to 2015.

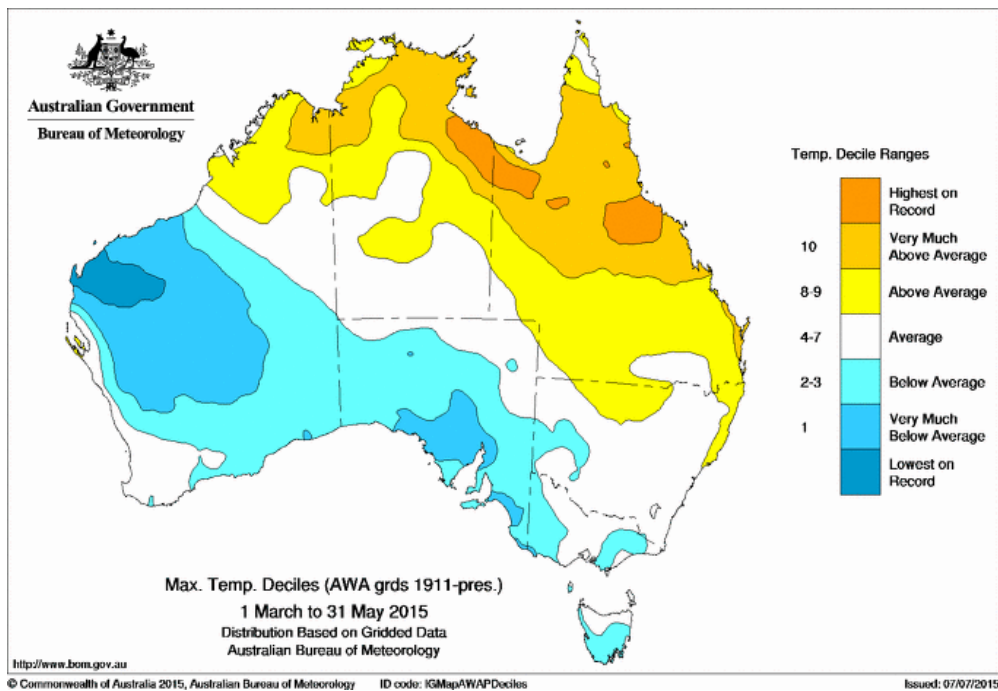


Figure 20 Autumn 2015 minimum temperature anomalies (°C).

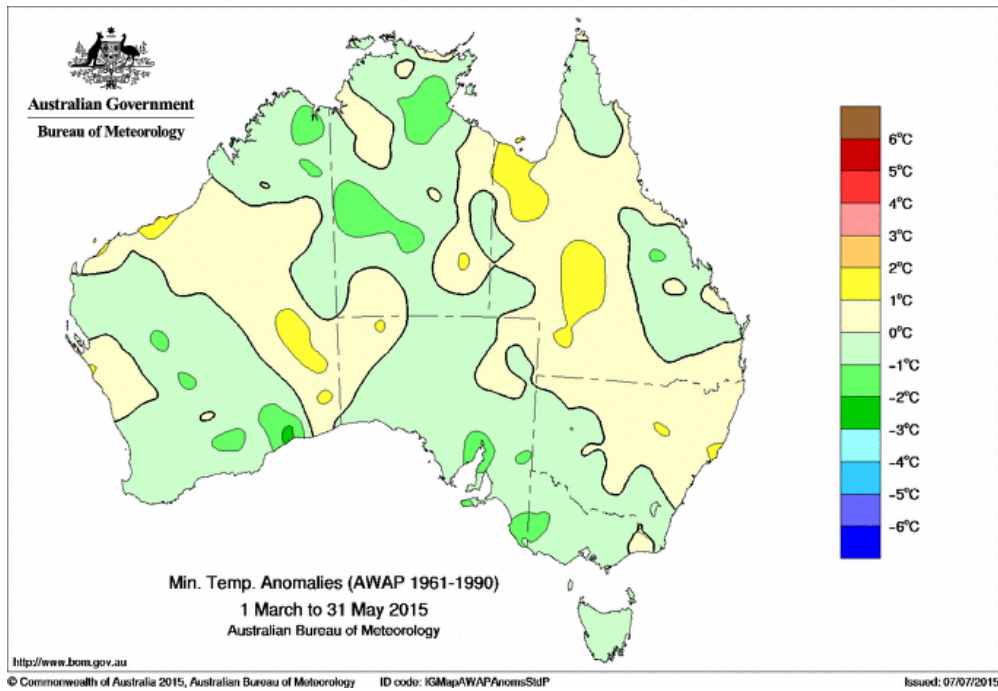
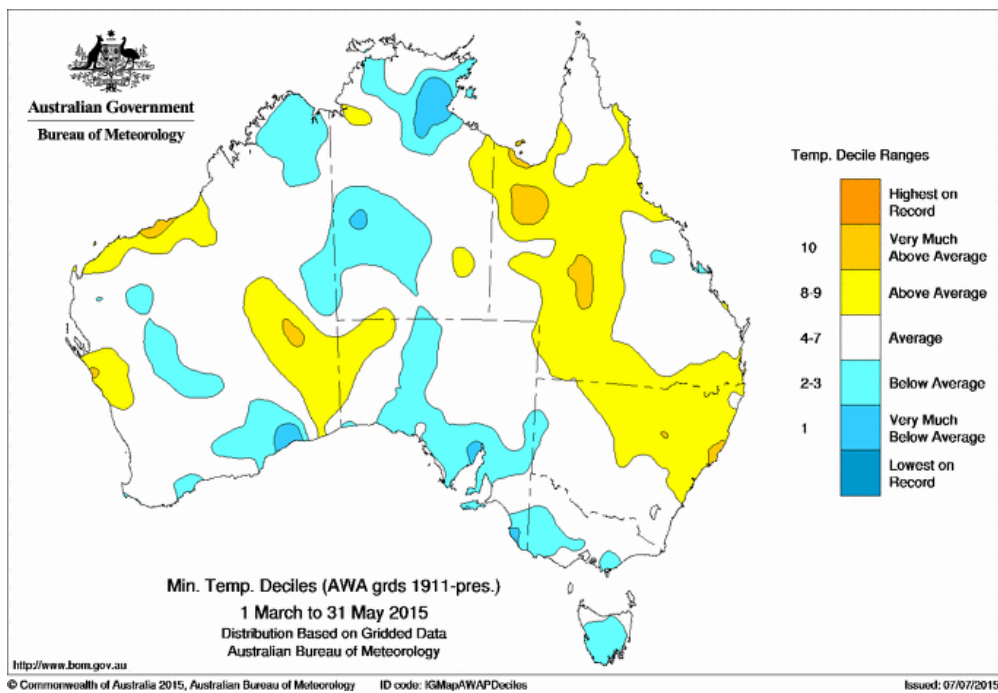


Figure 21 Autumn 2015 minimum temperature deciles: decile ranges based on grid-point values for all autumns from 1911 to 2015.



References

- Blockley, Y. 2015. Seasonal climate summary southern hemisphere (summer 2014-15): very warm summer with above average rainfall. *Aust. Met. Oceanogr. J.*, 65, 387-408.
- Cottrill, D.A. 2012. Seasonal climate summary southern hemisphere (spring 2011): La Niña returns. *Aust. Met. Oceanogr. J.*, 62, 179–192.
- Donald, A., Meinke, H., Power, B., Wheeler, M. and Ribbe, J. 2004. Forecasting with the Madden-Julian Oscillation and the applications for risk management. 4th International Crop Science Congress, 26 September – 1 October 2004, Brisbane, Australia.
- Hendon, H.H., Thompson, D.W.J. and Wheeler, M.C. 2007. Australian rainfall and surface temperature variations associated with the Southern Annular Mode. *J. Clim.*, 20, 2452–67.
- Hope, P., Reid, P., Tobin, S., Tully, M., Klekociuk, A., Krummel, P. 2015. Seasonal climate summary southern hemisphere (spring 2014): El Niño continues to try to break through, and Australia has its warmest spring on record (again!) *Aust. Met. Oceanogr. J.*, 65, 267-292.
- Kanamitsu, M., Ebisuzaki, W., Woollen, J., Yang, S.-K., Hnilo, J.J., Fiorino, M. and Potter, G.L. 2002. NCEP-DOE AMIP-II Reanalysis (R-2). *Bull. Am. Meteorol. Soc.*, 83, 1631–43.
- Kuleshov, Y. Qi, L., Fawcett, R., Jones, D. 2009. ‘Improving preparedness to natural hazards: Tropical cyclone prediction for the Southern Hemisphere,’ in: Gan, J. (Ed.), *Advances in Geosciences, Vol. 12 Ocean Science*, World Scientific Publishing, Singapore, 127–43.
- Madden, R.A., and Julian, P.R. 1971. Detection of a 40-50 day oscillation in the zonal wind in the tropical Pacific. *J. Atmos. Sci.*, 28, 702–708.
- Madden, R.A., and Julian, P.R. 1972. Description of global-scale circulation cells in the tropics with a 40-50 day period. *J. Atmos. Sci.*, 29, 1109–1123.
- Madden, R.A., and Julian, P.R. 1994. Observations of the 40-50 day tropical oscillation: a review. *Mon. Wea. Rev.*, 122, 814–837.
- Pepler, A. 2013. Seasonal climate summary southern hemisphere (winter 2012): dry conditions return to Australia. *Aust. Met. Oceanogr. J.*, 63, 339–349.
- Reynolds, R.W., Rayner, N.A., Smith, T.M., Stokes, D.C. and Wang, W. 2002. An improved in situ and satellite SST analysis for climate. *J. Clim.*, 15, 1609–25.
- Tobin, S. 2012. Seasonal climate summary southern hemisphere (winter 2011): a dry season in the lull between La Niña events. *Aust. Met. Oceanogr. J.*, 62, 97–110.
- Troup, A.J. 1965. The Southern Oscillation. *Quart. J. Roy. Meteor. Soc.*, 91, 490–506.
- Wheeler, M.C., and Hendon H.H. 2004. An All-Season Real-Time Multivariate MJO Index: Development of an Index for Monitoring and Prediction. *Mon. Weather Rev.*, 132, 1917–32.
- Wolter, K. and Timlin, M.S. 1993. Monitoring ENSO in COADS with a seasonally adjusted principal component index. *Proc. Of the 17th Climate Diagnostics Workshop*, Norman, OK, NOAA/NMC/CAC, NSSL, Oklahoma Clim. Survey, CIMMS and the School of Meteorology, Univ. of Oklahoma, 52–7.
- Wolter, K. and Timlin, M.S. 1998. Measuring the strength of ENSO – how does 1997/98 rank? *Weather*, 53, 315–24.